PCCP

Accepted Manuscript

ROYAL SOCIETY OF CHEMISTRY

www.rsc.org/pccp

PCCP

RSCPublishing

PAPER

Structures and optical properties for two phases of $SrMgF_4$

Cite this: DOI: 10.1039/x0xx00000x

Alexander P. Yelisseyev[1], Xingxing Jiang[2,3], Ludmila I. Isaenko[1,4], Lei Kang[2,3], Lei Bai[2], Zhushuai Lin[2,*], Alina A. Goloshumova[1], Sergei I. Lobanov[1], Dmitry Y. Naumov[5]

Received 00th January 2012,
Accepted 00th January 2012

DOI: 10.1039/x0xx00000x

www.rsc.org/

$SrMgF_4$ has an extremely large bandgap *Eg* of 12.50 eV as obtained from reflection dispersion. The symmetry of this crystal is monoclinic P21 at room temperature and transforms to orthorhombic Cmc21 phase near 478 K as temperature increases. Acentric character of the low-temperature (LT) phase is confirmed by pyroelectric luminescence at T < 440 K. The fundamental absorption edge of LT phase is located at 122 nm (10.15 eV). Considerable difference between absorption edge and bandgap *Eg* is due to the strong excition absorption. First-principles electronic structure, refraction indices, nonlinear susceptibility and polarizability were calculated for both LT and high-temperature (HT) phases. Band-to-band transitions are direct for LT phase but indirect for HT. In spite of relatively low birefringence (~ 0.017) and nonlinear susceptibility (~0.044 pm/V, an order lower than in KDP), $SrMgF_4$ crystals are considered promising for nonlinear optics thanks to their transparency far in the vacuum ultraviolet spectral region.

Introduction

The tetrafluoride of Sr and Mg ($SrMgF_4$, SMF) was synthesized for the first time 30 years ago[1, 2]. Banks et al[1] identified $SrMgF_4$ as orthorhombic. A negative test for second harmonic generation led them to suggest the space group *Cmcm* with *a*= 3.917(2), *b*=14.451(8) and c=5.637(2)[1]. It was surprising because all crystals in the isostructural Ba*M*F_4 (*M* = Mg, Mn, Fe, Co, Ni, Zn) family belong to a pyroelectric symmetry class *Cmc*2_1. Some of Ba*M*F_4 compounds were observed to undergo phase transitions of different nature[3-5]. These materials are unique for optical applications in the vacuum ultraviolet (VUV) to mid-IR spectral range because of combination of nonlinear optical (NLO) properties with a wide transparency range from 125 nm to 13 μm[3]; birefringent effects and quasi-phase-matching were demonstrated in $BaMgF_4$[3]. Later detailed X-ray structural studies on SMF established its monoclinic symmetry *P*112_1 at low temperature with parameter ***a*** doubling and ***c*** tripling[6] compared with the orthorhombic *Cmcm* previously reported in the literature[1].

A possible existence of the structural phase transition in the SMF crystal was discussed[2,6,7]. The presence of local mirror planes in the superstructure of Sr atoms at low temperature allowed one to suppose the existing of the high-temperature phase[6]. This possibility was also suggested taking into account the thermal abnormality of SMF near 1082 K in differential thermal analysis data[1], whereas its melting temperature is of about 1153 K. On the basis of X-ray structural data[6], Abrahams *et al* showed that this crystal meets the structural criteria of ferroelectricity[7]. They predicted the value of spontaneous polarization at room temperature ($P_s \approx 11 \cdot 10^{-2}$ C m^{-2}), which is typical of 2D ferroelectrics, and phase transition to paraelectric state near T_c = 450 K with the symmetry change: *P*2_1 (Z = 12) ↔ *P*$2_1/m$ (Z = 12)[7]. Recent polarization-optical observations and preliminary X-ray structural studies in the 90 to 1200 K range for $SrMgF_4$ crystal revealed a non-intrinsic ferroelastic phase transition with *P*112_1 (Z = 12) ↔ *Cmc*2_1 (Z = 4)[8], and both phases remain pyroelectric, in contrast to the results by Abrahams[7]. In addition, the SMF reflection and photoluminescence were studied in detail using the synchrotron radiation[9] and its energy band gap was estimated to be E_g = 12.50 eV. To date there are no experimental data concerning the fundamental absorption edge of $SrMgF_4$, as well as its electronic structure and nonlinear susceptibility.

In the present work the sizable SMF single crystals were obtained, and the structures for both low-temperature (LT) and high-temperature (HT) phases were determined. The pyroelectric luminescence measurements confirmed that LT phase is noncentrosymmetric. The transmission spectrum for LT phase of SMF was recorded and the absorption edge was found to be 122 nm (10.15 eV). Its red-shift in comparison with E_g = 12.50 eV[9] is a result of strong excitonic absorption. The electronic structures, refractive indices, nonlinear susceptibility and polarizability were calculated by first-principles theory for both LT and HT phases.

Results and discussion

In this work the structures of both LT and HT phases for SMF were accurately determined for the first time.

Structures of LT and HT SMF phases

Low-temperature SMF phase (Fig. 2a). At room temperature a monoclinic ***P2$_1$*** structure with doubled ***a*** and tripled ***c*** cell lengths compared with the orthorhombic ***Cmcm*** structure reported in Ref. 1 was established. Lattice parameters are: *a*=7.4736 Å, *b*=16.8835 Å, *c*=7.8010 Å, *β*= 105.0302°, V=950.66 Å^3, *Z*=12, $D_{calc.}$= 3.9383 g/cm^3.In the $SrMgF_4$ structure there are 6, 6 and 24 unequivalent positions for strontium, magnesium and fluorine ions. The structure can be described as a lamellar one; perpendicular lines to the layers are in the *a*-*b* plane. These layers are composed of chains, which are drawn along ***b*** axis and consist of irregular corner-sharing MgF_6 octahedra, rotated relative to each other (Fig. 2a). The perovskite-type slabs, composed of corner-sharing MgF_6 octahedra and Sr atoms, are stacked along the ***b*** axis. Six crystallographically independent MgF_6 octahedra are rotated so as to provide long periodicities along ***a*** and ***c***. The coordination numbers and bond distances around the six crystallographically independent Sr atoms are slightly different in each case. In the superstructure, the Sr atoms lie in local mirror planes which are thought to originate at the high-temperature phase transition[6]. Strontium ions are situated between the layers and depending on their position are surrounded by 7 (Sr1, Sr2), 9 (Sr3, Sr5) or 10 (Sr4, Sr6) fluorine ions (Fig. **3**). Coordination numbers were estimated by the construction of Dirichlet polyhedra using Xshell software. The bond lengths for Sr ions are represented in Table 1.;The structure of the LT Phase is in good agreement with that published earlier in Ref. 6 for Ce-doped $SrMgF_4$.

High-temperature SMF phase (Fig. 2b). At temperatures above 205ºC (478 K) there is some ordering in the SMF lattice. It is described by an orthorhombic symmetry $Cmc2_1$ with lattice parameters *a*=3.9369 Å, *b*=14.4884 Å, *c*=5.6379 Å, V=321.58 Å^3, *Z*=4, $D_{calc.}$=3.8808 g/cm^3. Similarly to the LT phase this structure can be described as a lamellar one. However this time the chains of irregular MgF_6 octahedrons are extended along the ***c*** axis and join in tops, forming the layers oriented parallel to the crystallographic (010) plane. The fluorine ions occupy 4 nonequivalent sites whereas both Sr and Mg ions have only one position each. The simulated XRD data for HT phase are given Fig. S1 in SI section.

Pyroelectric luminescence (PEL)

SMF crystals demonstrate a spontaneous emission in the 80 to 440 K range as temperature changes (both at cooling and heating) on sample at rate β = dT/dt about 20 K/min (Fig. 4). Such emission is typical only for pyroelectrics and is interpreted as a result of the modification in atomic polarization on crystal surface or in its volume due to the change in temperature[10]. The strength of pyroelectric field can reach tens of kV. It is interesting that both onset temperatures at which PEL disappears (at heating) and appears (at cooling) are close to that for LT ←→ HT phase transition in SMF. The occurrence of PEL in SMF indicates that there is no symmetry center at T < 440 K which agrees the results of structural analysis. Since the HT phase remains noncentrosymmetric, PEL absence at T>478 K in SMF is supposed to be the result of much smaller pyroelectric coefficient γ above this temperature.

We have also observed the PEL effect in typical NLO crystals such as $LiIO_3$, β-BaB_2O_4 (BBO), LiB_3O_5 (LBO), Ag_3AsS_3, $LiNbO_3$, $LiGaS_2$, and KTP[11]. Main features of their PEL spectra are listed as follows[10]:

1. PEL intensity lowers as the size of pyroelectric crystals decreases. PEL disappears completely when the crystal size becomes smaller than 1 mm. The charge *Q* on the opposite faces of pyroelectric crystal is proportional to sample volume (~R^3), whereas distance between these faces is proportional sample diameter (*R*). As a result the intensity E of pyroelectric field is roughly proportional to R^2 and falls quickly in line with the electric break-down probability as *R* decreases. The other reason may be the leak of the charge along the defect states in the near-surface layer: its efficiency also increases as sample becomes smaller.
2. The intensity and frequency of PEL pulses depend considerably on the rate of temperature

increase/decrease β. Both intensity and frequency decrease as β falls.

3. PEL is most intense in the temperature ranges with maximal values of pyroelectric coefficient γ. Thus, in $LiIO_3$ near 140 K the pyroelectric coefficient is $\gamma = 5\times10^{-5}$ coulomb·m^{-2} K^{-1}, which is 5 times higher than at room temperature[11]. Indeed, PEL is observed at low temperatures but it disappears at T>200 K. Special measurements showed that PEL takes place also near 570 K in $LiIO_3$ which corresponds to a sharp γ maximum in the α→β phase transition.
4. PEL weakens up to be completely disappeared near room temperature in the Li-containing crystals as the increase of Li^+ ionic conductivity suppresses the generation of pyroelectric field.
5. Shining with X-ray and photoexcitation during heating/cooling or at low temperature before heating can heavily suppress PEL: the temperature range where PEL takes place becomes narrower or PEL disappears completely.

Optical transmission

Transmission spectrum for LT phase of $SrMgF_4$, recorded at 300 K using three different spectrometers, is given in Fig. 5; it covers all the transparency range from VUV to mid-IR. One can see in the insert that a shortwave edge of fundamental absorption is located at 122 nm (hν =10.15 eV) on the 0 transmission level and there are no noticeable spectroscopic features to the long-wave edge at 11.8 μm. Taking into account that Raman spectrum of SMF covers the 100 to 450 cm^{-1} range in the wave number scale, we suppose that IR limit is due to the two-phonon absorption. Unfortunately, there are several slightly pronounced shoulders in the VUV region. Additional absorption bands near the fundamental absorption edge are more pronounced in the insert with the extended scale. The UV absorption spectrum can be decomposed into 4 components, as shown in Fig. 6. We separated four Gaussian components with maximums at 6.3, 7.65, 9.1 and 10.05 eV, which have the full widths at the half-maximum FWHM = 1.8, 1.2, 1.4 and 0.72 eV, respectively: These bands are likely be attributed to the electronic transitions in some point defects such as vacancies or cation antisite defects. Taking into account the ionic radii of cations (0.86 A and 1.27 A for Mg^{2+} and Sr^{2+} in fluorine environment[12], respectively), it is expected that the dominant antisite defects are small Mg ions occupied at the large Sr sites (Mg_{Sr}).We suppose that the SMF transparency will be improved if the concentration of corresponding defects lowers. For crystals of multicomponent compounds this happens usually when crystal composition is close to the stoichiometric one[13]. Rapid increase of absorption is observed only at hν >10 eV.

Photo-and X-ray excited luminescence

An intense luminescence with photon energies in the range from 1 to 6 eV is observed in photoluminescence (PL) spectra. Typical PL spectra at 10.6, 10.9 and 3.8 eV excitations are shown by curves 1-3 in Fig. 7a in comparison with spectrum of X-ray excited luminescence (XL, curve 4). The photoluminescence excitation (PLE) spectra for 3.1 and 4.8 eV emissions are given in Fig. 7b. PL spectra 1-2 and PLE spectra 5-6, recorded for LT phase of SMF at 10 K using the synchrotron radiation are taken from Ref. 9. PLE spectra demonstrate intense relatively narrow bands in the 10-11.5 eV range and a weaker band near 11.8 eV. Such spectra are typical of excitonic excitations in the wide-gap dielectrics $BaMgF_4$[14], SrF_2[15], MgF_2[16]. Narrow PLE bands are somewhat shifted to low energies in comparison with excitonic peak in reflection and absorption spectra: the latter has maximum near 11.4 eV in the spectrum (7). The profile of the dominating 10.7 eV PLE band is caused by two competitive processes. The low-energy slope of this band is determined by absorption/excitation increase whereas the high-energy negative slope is due to surface energy losses. Intensity of the excitonic absorption peak is high (about 10^6 cm^{-1}) and just absorption in its low energy wing determines the fundamental absorption edge. Transmission spectrum calculated for a 1 mm thick SMF plate taking into account only exciton aborption, with zero absorption of point defects, is shown as curve 4 in Fig. 5. Thus, the calculated absorption edge was predicted to be 10.5 eV [9] which is close to experimental 10.15 eV value in present paper. Difference between these values can be partly explained by temperature effect: transmission was measured at room temperature whereas reflection spectra have been recorded at T = 10 K in Ref. 9. Experimental absorption edge is expected to shift about 0.2 eV if to lower the sample temperature and the agreement would be better. PLE and calculated absorption spectra for SMF agree well at assumption concerning surface losses of energy and diffusion of electronic excitations (EE) in SMF, the length of EE diffusion being 70 nm [9]. PL emission in the 3.5-4.6 eV range (the 3.7 and 4.2 eV bands) is excited in the exciton band 10.7 eV with a shoulder near 11.0 eV (components C and D in terms of Ref. 9). PL in the 5.0 eV band is excited in the 10.5 eV band (B-

component). Taking into account that both these PL emissions are excited only in the exciton bands near the absorption edge and the Stokes shift for them is large (about 6.5 eV), they may be related to self-trapped excitons[17]. As follows from spectrum (3) in Fig. 7a, the low-energy PL in the 2 to 3.5 eV range (bands at 2.45, 2.67 and 2.0 eV) can be excited effectively by the 3.8 eV light from the SMF transparency range as well as in the 6.0 eV band[9]. Main part of these emissions is excited also by the X-rays: in this case hot charge carriers thermalize with further EE transfer both to excitons and point defects (see (4) in Fig. 7a). The low-energy PL emissions can be associated with radiative recombination in some non-identified point defects: they may be color centers based on anion vacancies, structural defects in cation sublattices as well as impurity defects. The variety of features in the PL and PLE spectra may be due to different nonequivalent positions for each ion (6, 6 and 24 for strontium, magnesium and fluorine ions, respectively, in the $MgSrF_4$ structure). Such crystallographically nonequivalent positions differ in coordination number, bonds length, and in intensity of the crystal field.

The presence of intense excitonic bands near the absorption edge makes the analysis of the edge shape and exact determination of the E_g values from optical transmission difficult. SMF crystals belong to the SrF_2-MgF_2 system. Binary components of this system crystallize in the cubic fluorite (SrF_2) and tetragonal rutile (MgF_2) structures[2]. Although the SMF structure is formally different from that of SrF_2 and MgF_2, its electronic structure should inherit some features of the binary compounds. In terms of the SMF structure, the main translational motive in SMF is a continuous network of MgF_2 octahedrons. Comparison of optical constants for SrF_2, MgF_2 and $MgSrF_4$ shows that values for the latter are between the parameters for binary compounds. Indeed, the E_g values for E || c and E⊥c polarizations in MgF_2 are 12.8 and 13.4 eV, respectively, whereas for SrF_2 band gap is about 1 eV narrower: 11.25 and 11.44 eV, according to different authors[9]. Excitonic absorption peaks are located at 10.6 and 12.1 eV for SrF_2 and MgF_2, respectively, in comparison with E_g=11.4 eV in SMF. High energy edge of the fundamental absorption is considerably shifted to lower energies: 9.5 and 11 eV for SrF_2 and MgF_2[9], respectively, whereas for SMF it is 10.15 eV. Considerable difference between absorption edge and E_g takes place also in NLO crystal BBO[9]: absorption edge is located near 6.2 eV and band gap for direct Γ-Γ transition is 7.5 eV: their difference is due to intense excitonic absorption in the boron-oxygen group as well as to the charge transfer transitions O-Ba[18,19].

First-principles results

Based on the obtained structural data (ESI), the electronic structures were calculated for LT and HT phases of SMF. The density of states (DOS) and partial density of states (PDOS) projected on atom species are plotted in Figs. 8a and 8b, and show the very similar electronic characteristics in both phases. The Sr 4s and 4p orbitals are located at -29 eV and -12 eV, respectively, while the F 2s orbitals are located at -20 eV. All electrons originally on the Mg 3s and Sr 5s shell are almost lost and move into the F 2p shell, which dominantly occupy the top of valence band. All orbitals are quite localized and there is a very weak hybridization indicating that the chemical bonds between the constituent atoms are almost ionic rather than covalent.

The electronic band structures for low-T and high-T phases along the lines of high symmetry points in the Brillouin zone of $MgSrF_4$ are shown in Fig. 9a and 9b, respectively. The states density in LT phase is much higher than that in HT phase since Z=12 for the former and Z=4 for the latter. One can see that direct electronic transitions in the Γ point are responsible for the fundamental absorption edge for the LT phase, but there are indirect Σ→Γ transitions for the HT phase and the direct gap at Γ point is about 0.09 eV larger than the indirect one. The calculated bandgap energies of the LT and HT phases are 6.64 eV and 6.74 eV, respectively. The discrepancy between calculated and experimental values is due to the notorious bandgap prediction problem by density functional theory. However, the relative magnitude of bandgap energies can be determined from the DFT values for the similar system. Thus, it is predicted that the LT and HT phases actually have close bandgap energies.

In order to elucidate the difference of pyroelectric behaviors in the LT and HT phases of SMF, the response of the materials to an applied electric field, i.e., the polarizabilities were calculated. The matrices of polarizability tensors for the dynamic (optical, $\omega = \infty$) and static ($\omega = 0$) electric fields are listed in Table 2. Clearly, both dynamic and static polarizability are considerably (6 to 12 times) larger for the LT phase of SMF. Our calculated results are consistent with the fact that the LT phase is less ordered in comparison with HT: this originates from the larger distortion of the Mg position from the gravity center of MgF_6 octahedron in the former phase. This conclusion agrees with the predictions of Abrahams[7] concerning relatively high

spontaneous polarization (~10 μC/m^2) for SMF at room temperature as well. More importantly, this result also confirms that the PEL phenomenon in SMF is much more evident at low temperatures (Fig. 3) since larger pyroelectricity is often accompanied by larger polarizability[20]. Consequently, it is of great importance to measure polarization experimentally and confirm ferroelectric properties of SMF. If SMF is related to ferroelectrics it is possible to change direction of the spontaneous polarization vector using an external electric field and realize the quasi-phase matching (QPM) regime as in the case of potassium titanyl phosphate $KiTiOPO_4$ (KTP) or lithium niobate $LiNbO_3$ (LN) [21].

Table 2 lists the calculated values of refractive indices n_i and birefringence Δn, at 523 and 1064 nm as well as the static SHG coefficient in SMF. For both phases the refractive indices vary in the 1.42-1.44 range and birefringence is 0.016-0.018. Previous Kramers-Krönig transform analysis gave 1.4464, 1.621 and 1.632 for MgF_2, SrF_2[15] and $SrMgF_4$[9] at 7.87 eV. Since n_i decreases in line with photon energy, our calculated values are consistent with these results. Moreover, the calculated Δn values agree well with the available experimental data[8]. The Δn values for SMF are 2.5 to 3 times smaller in comparison with the widely-known NLO crystals for VUV-UV-visible range (see Table S1 in the supplementary information). The maximum components of SHG coefficients d_{ij} are 0.044 pm/V for LT, 2 times higher than that for HT (0.021 pm/V). However, even this value is very small; it is an order lower than that of KDP and about 2 orders lower than that of BBO (Table 2). Nevertheless, SMF may be promising for VUV NLO applications thanks to its transparency down to 122 nm (or E_g ~ 10.15 eV), shorter than those in almost all known commercial NLO crystals used in the VUV (see Table S1).

To date $BaMgF_4$ is the most studied from the SMF relatives. It has the same $Cmc2_1$ structure as HT SMF; small Δn~0.02 and d_{ij} (0.015 to 0.039 pm/V) values. BMF is transparent in the 0.125-13 μm range and is ferroelectric with the 4 kV/cm coercive field, and its QPM was realized for SHG [3,4]. For the LT phase of SMF calculated nonlinearity is slightly larger and transparency range slightly wider in VUV compared with $BaMgF_4$, so the studies of QPM on SMF is of great importance.

Conclusions

We have obtained the sizable $SrMgF_4$ single crystals and determined the structures of LT and HT phases. Intense pyroelectric luminescence at T<440 K confirms absence of symmetry center for LT phase. Transmission spectrum for LT phase of SMF was measured and shortwave fundamental absorption edge was established at 122 nm (10.15 eV). Its considerable shift in comparison with bandgap value (12.5 eV) is explained by strong excitonic absorption.

Electronic structure was calculated for LT and HT phases of SMF, type of band-to-band transitions was established: direct Γ→Γ for LT and indirect, Σ→Γ, for HT. Energy band gap values for these SMF phases were found close each other.

Main optical parameters for SMF were calculated: refractive indices, birefringence, nonlinear susceptibility. LT phase has higher nonlinear susceptibility, but it is still 1 and 2 order lower than that in KDP and BBO, respectively. Several times higher polarizability for low-symmetry LT phase allows one to explain why pyroelectric luminescence is observed only for this phase in SMF crystals.

Experimental and computational details

Crystal growth

The $SrMgF_4$ synthesis was carried out from the mixture of fluorides SrF_2 and MgF_2 at temperature 1670 K in presence of fluoride agent (CF_4). To remove oxygen–containing impurities the starting chemicals were annealed in the dynamic vacuum during 24 h at 770 K. A glass-graphite crucible with a conic bottom was filled with synthesized substance and placed into a silica hermetically sealed ampoule evacuated to 10^{-1} Pa pressure. Crystals were grown using the Bridgman technique in a two-zone furnace with temperatures 1470 K and 970 K in different zones. The rate of the ampoule sinking was about 1mm/day, whereas temperature gradient in the growth area was 10 to 20 K/cm. Crystal was cooled in the regime of the switched-off furnace. The obtained transparent colorless crystals of about 1 cm^3 in volume (Fig. 1) were obtained after annealing in vacuum during a day.

Crystal structure

Pure and optically transparent single crystal 0.19×0.13×0.11 mm^3 in size was used for the X-ray structural study. Investigation was carried out on a Bruker APEX DUO diffractometer (Mo*Kα*-radiation, graphite monochromator, CCD detector) in the 2.41 to 28.28^o angle θ range {Bruker AXS Inc. (2004), APEX (Version 1.08), SAINT (Version 7.03) and SADABS (Version 2.11) Bruker Advanced X-Ray Solutions. – Madison, Wisconsin, USA}. All structure

determinations were carried out using software SHELX [22, 23]. For crystal structure analyses we used Xshell program[24, 25]. Graphics visualizing of the structures was made via BS program (Balls&Sticks ver. 1.42 by Sung J. Kang & Tadashi C. Ozawa). SMF structure was studied at room temperature and 550 K. Sample was heated by a directed hot air flow. As a result we confirmed that there are two different phases below and above the phase transition at 478 K[8].

Spectroscopic studies

Transmission spectra were recorded using a UV-2501PC Shimadzu spectrometer in the UV – to-near IR, whereas in the mid-IR we used a Fourier-Transform spectrometer Infralum 801. The VUV transmittance spectrum was recorded using a McPherson Vacuum UV Analytical Spectrophotometer VUVAS 2000 spectrometer. The photoluminescence (PL) spectra were measured using a LabRam microRaman spectrometer at 325 nm excitation from a He-Cd laser. X-ray excited luminescence (XL) was recorded with a MDR2 diffraction monochromator with photomultipliers FEU100 and cooled FEU83 as emission detectors; a table 1 kW X-ray set-up was used for excitation. Pyroluminescence (PLE) was recorded as a spontaneous emission from the pyroelectric crystal both at its heating or cooling at a rate of about 20 K/min in the temperature range from 100 K to 550 K: we used a FEU100 photomultiplier.

First-principles computational methods

The first-principles calculations were performed by CASTEP[26], a plane wave pseudo potential total energy package based on density functional theory (DFT)[27]. The exchange-correlation functional developed by Ceperley, Alder[28], Perdew and Zunger[29] (CA-PZ) of local density approxiamtion (LDA)[30] form was adopted. The optimized norm-conserving pseudopotential[31] in Kleinman-Bylander[32] form allow us to use a relatively small basis set without compromising the computational accuracy, and the Sr $4s^2 4p^6 5s^2$, Mg $3s^2$ and F $2s^2 2p^5$ are treated as the valence electrons. Kinetic energy cutoff of 900eV and Monkhorst-Pack[33] k point mesh of 7×7×4 and 3×1×3 were chosen for HT and LT phases, respectively. Our tests showed that the computational parameters above are accurate enough for the present purpose.

Based on the electronic structures, the optical refractive indices and SHG coefficients for the LT and HT SMF crystals were determined from the virtual electronic transitions between the valence and conduction bands[34, 35]. The polarizabilities in the LT and HT SMF crystals were obtained by the linear response method in the density-functional perturbation theory[36], in which the polarizability is calculated through computing the second derivative of the total energy with respect to a given perturbation in ionic positions.

Acknowledgements

This work was partly supported by the Ministry of Education and Science of the Russian Federation, the National Natural Science Foundation of China under Grant Nos 11174297 and 91022036, and the National Basic Research Project of China (Nos 2010CB630701 and 2011CB922204).

Notes

[1]Institute of Geology and Mineralogy, Siberian Branch of the Russian Academy of Sciences, 3 Ac.Koptyug ave, Novosibirsk 630090, Russia.
[2]BCCRD, Key Laboratory of Functional Crystals and Laser Technology, Technical Institute of Physics and Chemistry, Chinese Academy of Sciences, , Beijing 100190, China.
[3]University of Chinese Academy of Sciences, Beijing 100049, China.
[4]Novosibirsk State University, 2 Pirogova str., 630090, Novosibirsk, Russia.
[5]Institute of Inorganic Chemistry, Siberian Branch of the Russian Academy of Sciences, 3 Ac. Lavrentyev ave, Novosibirsk 630090, Russia

*Corresponding author, email: zslin@mail.ipc.ac.cn

Electronic Supplementary Information (ESI) available: Simulated XRD for LT and HT $SrMgF_4$ phases;
CIF file of LT and HT phases of SMF and main optical properties for wide-band NLO crystals (Table S1). See DOI: 10.1039/b000000x/

Reference.

1 E., Banks, S. Nakajama, M. Shone, New Complex Fluorides $EuMgF_4$, $SmMgF_4$, $SrMgF_4$, and Their Solid Solutions: Photoluminescence and Energy Transfer. *J. Electrochem. Soc.,* 1980, 127, 2234-2239.
2 O. Bingyi, E. Banks, Binary System SrF_2-MgF_2: Phase Diagram and Study of Growth of $SrMgF_4$, *Mater. Res. Bull.,* 1982, 17, 1185-1188.
3 E. G. Villora, K. Shimamura, K. Sumiya, H. Ishibashi, Birefringent- and Quasi-Phasematching with $BaMgF_4$ for VUV and Mid-IR All Solid State Lasers, *Opt. Express* , 2009, 17, 12362-12378.

4 J. F. Scott, Phase Transitions in $BaMgF_4$, *Rep. Prog. Phys*., 1979, 12, 1055-1084.
5 R. V. Pisarev, B. B. Krichevtzov, P. A. Markovin, O. Y.Korshunov, Scott, J. F. Optical Phenomena in $BaMnF_4$ Near Its Phase Transition. *Phys. Rev. B ,*1983, 28, 2677-2685.
6 N. Ishizawa, K. Suda, B. E.Etschmann, T. Oya, N. Kodama, Monoclinic Superstructure of $SrMgF_4$ with Peroskite-type Slabs. *Acta Cryst.,* 2001, C57, 784-786.
7 S. C. Abrahams, Structurally Ferroelectric $SrMgF_4$. *Acta Cryst*., 2002, B58, 34-37.
8 S.V. Melnikova, L. I. Isaenko, A. A. Goloshumova, S. I. Lobanov, Investigation of the Ferroelastic Phase Transition in the SrMgF4 Pyroelectric,*Crystal. Phys. Sol. State*,2014,56,757-760
9 I. N. Ogorodnikov, V. A. Pustovarov, S. I. Omelkov, L. I. Isaenko, A. P. Yelisseyev, A. A. Goloshumova, S. I. Lobanov, A Far Ultraviolet Spectroscopic Study of the Reflectance, Luminescence and Electronic Properties of $SrMgF_4$ Single Crystals. *J. Lumin.*, 2014, 145, 872-879.
10 A. P. Yelisseyev, L. I. Isaenko, M. K. Starikova, Luminescence in Lithium Iodate α-$LiIO_3$. *JOSA*, B 2012, 29, 1430-1435.
11 D. N. Nikogosyan, *Nonlinear Optical Crystals: A Complete Survey*, Springer, 2005.
12 R.D. Shannon, C.T. Prewitt, Effective ionic radii in oxides and fluorides. *Acta Crystallogr.,* 1969, B25, 925-946.
13 A. Yelisseyev, Z. S. Lin, M. Starikova, L. Isaenko, S. Lobanov, Optical transitions due to native defects in nonlinear optical crystals $LiGaS_2$ *J. Appl. Phys.* 2012. 111**,** 113507.
14 S.C.Buchter, T. Y.Fan, V. Liberman, J. J. Zauhovky, M. Rothshild, E. J. Mason, A. Cassanho, H. P. Jenssen, Periodically Poled $BaMgF_4$ for UV Frequency Generation. *Opt. Lett*., 2001, 27, 1693-1695.
15 T. Tomiki, T. Miyata, Optical Studies of Alkali Fluorides and Alkaline Earth Fluorides in VUV Region. *J. Phys. Soc. Jpn*. ,1969, 27, 658-678.
16 M. W. Williams, R. A. MacRae, E. T. Arakawa, Optical Properties of Magnesium Fluoride in the Vacuum Ultraviolet. *J. Appl. Phys.,* 1967, 38, 1701-1705.
17 A. K. S. Song, R. T.Williams, *Self-Trapped Excitons,* Springer Verlag, Berlin-Heidelberg, N.Y.: 1996.
18 V.Kisand, R. Kink, M. Kink, J. Maksimov, M. Kirm, Martinson, I. Low-Temperature Optical Spectroscopy of Nonlinear BBO Crystals., *Phys. Scripta.,*1996, 54, 542-544.
19 W. D. Cheng, J. S. Huang, J. X. Lu, Electronic Structures and Nonlinear Optical Coefficients of β-BaB_2O_4. *Phys. Rev. B,* 1998, 57, 1527-1533.
20 M. Roessle, K. W. Kim, A. Dubroka, P. Marsik, C. N.Wang, R. Jany, C. Richter, J. Mannhart, C. W. Schneider, A. Frano, P. Wochner, Y. Lu, B. Keimer, D. K. Shukla, Strempfer, J., Bernhard, C. Electric-Field-Induced Polar Order and Localization of the Confined Electrons in $LaAlO_3/SrTiO_3$ Heterostructures. *Phys. Rev. Lett.,* 2013, 110, 136805.
21 V. S. Pasiskevicius, S. Wang, J. A. Tellefse, F. Laurell, H. Karlsson, Efficient Nd: YAG Laser Frequency Doubling with Periodically Poled KTP. *Appl. Opt. ,*1998, 37, 7116-7119.
22 G.M. Sheldrick, *SHELX97 Release 97-2*, University of Gottingen, Germany, 1998
23 G.M. Sheldrick, A short history of SHELX. *Acta Crystallogr. A,* 2008, 64, 112.
24 D.Y. Naumov, E.V. Boldyreva, Software for localization and visualization of cavities in crystal structures and supramolecular assemblies. *Russ. J. Stuct. Chem.*, 1999, 40, 86-93.
25 N. E. Kashcheeva, D. Y. Naumov, E. V. Boldyreva, Software for calculating Dirichlet domains and examples of its application for the analysis of crystal structures of cobalt(III) nitropentaammines. *Z. Kristallogr.*, 1999, 214, 534-541.
26 S. J. Clark, M. D. Segall, C. J. Pickard, P. J. Hasnip, M. J. Probert, K.Refson, M. C. Payne, First Principles Methods Using CASTEP. *Z. Kristallogr.*, 2005, 220, 567-570.
27 W. Kohn, L. J. Sham, Self-Consistent Equations Including Exchange and Correlation Effects. *Phys. Rev.*, 1965, 140, A1133-A1138.
28 D. M.Ceperley, B. J. Alder, Ground-State of the Electron-Gas by a Stochastic Method. *Phys.Rev. Lett*., 1980, 45, 566-569.
29 J. P. Perdew, A. Zunger, Self-Interaction Correction to Density-Functional Approximations for Many-Electron Systems. *Phys.Rev. B*, 1981, 23, 5048-5079.
30 R. G. Parr, S. R. Gadre, L. J. Bartolotti, Local Density Functional Theory of Atoms and Molecules. *Proc. Natl. Acad. Sci*. ,USA. 1979, 76, 2522-2526.
31 A. M. Rappe, Rabe, K. M. Kaxiras, J. D Joannopoulos,. Optimized Pseudopotentials. *Phys.Rev. B*, 1990, 41, 1227-1230.

32 L. Kleinman, D. M. Bylander, Efficacious Form for Model Pseudopotentials. *Phys.Rev. Lett.,* 1982, 48, 1425-1428.
33 H. J. Monkhorst, J. D. Pack, Special Points for Brillouin-Zone Integrations. *Phys. Rev. B,* 1976, 13, 5188-5192.
34 J. Lin, M. H. Lee, Z. P. Liu, C. T. Chen, C. J. Pickard, Mechanism for Linear and Nonlinear Optical Effects in Beta-BaB_2O_4 crystals., *Phys.Rev. B*, 1999, 60, 13380-13389.
35 Z. S. Lin, J. Lin, Z. Z.Wang, Y. C.Wu, N. Ye, C. T.Chen, R. K. Li, Theoretical Calculations and Predictions of the Nonlinear Optical Coefficients of Borate Crystals. *J. Phys.: Condens. Matter*., 2001, 13, R369-R384.
36 S. Baroni, S. de Gironcoli, A. Dal Corso, P. Giannozzi, Phonons and Related Crystal Properties from Density-Functional Perturbation Theory. *Rev. Mod. Phys.,* 2001, 73, 515-562.

Table Captions

Table 1. Selected bond lengths [Å] for Sr atoms in LT and HT $SrMgF_4$ structures

Table 2. *Ab initio* calculated linear (refractive indices, birefringence) and nonlinear optical (SHG coefficients) properties for LT and HT phases of SMF.

Table 3. The spontaneous dipole moment and components of the polarizability tensor α_{ij} for different phases of $MgSrF_4$ (10^{-24} cm^3)

Figure Captions

Fig.1. Single crystal $MgSrF_4$ sample, 2 mm thick.

Fig.2. The structure of $SrMgF_4$: low-temperature (a) and high-temperature (b) phases. Green spheres are Sr ions located among the MgF_6 polyhedrons. Different color of MgF_6 octahedrons in section (a) shows that they are turned each other and are crystallographically nonequivalent.

Fig.3. The coordination of Sr ions in LT and HT $SrMgF_4$ structures.

Fig.4. Spontaneous emission (PEL) in SMF crystals at heating (a) and cooling (b). Heating / cooling rate β is about 20 K/min.

Fig.5. Transmission spectrum in the VUV to near IR spectral range for a low-temperature MSF phase at T=300 K. d=1.2 mm. In the insert: Detail in the shortwave range for SMG plates 0.5 mm and 1.2 mm thick: curves 2 and 3, respectively. 4-shows transmission spectrum for 1 mm thick SMF plate, reconstructed from the reflection spectrum supposing only excitonic absorption near the fundamental absorption edge, without any features related to defects.

Fig.6**.** Decomposition of the room-temperature absorption spectrum for LT-SMF near the fundamental absorption edge: there are 4 gaussians centered at 6.3, 7.65, 9.1 and 10.05 eV (curves 1-4) whereas (5) shows an intense edge absorption.

Fig.7. (a) PL spectra for LT phase of $SrMgF_4$ at 10.6 eV (1), 10.8 eV (2) and 3.8 eV (3) excitations. The XL spectrum is given for comparison (4). (b) PLE spectra for 3.6 eV and 5.0 eV emissions are shown by (5) and (6) curves, respectively. Spectra 1-2, 5-6 are taken from [10]. Absorption spectrum (7) was reconstructed from the reflection spectrum in [10]. Spectra (1-2, 5-6) were recorded at 10 K, whereas spectra (3, 4) were obtained at 300 K. The arrow shows the band gap E_g=12.5 eV in SMF.

Fig.8. DOS and PDOS projected on constitutional species of atoms in (a) LT phase and (b) HT phase of $SrMgF_4$ (Unit: electrons/eV). The vertical dashed lines indicate the valence band maximum.

Fig.9. Comparison of the electronic band structure along the lines of high symmetry points in the Brillouin zone for (a) LT phase and (b) HT phase of $SrMgF_4$.

Table 1. Selected bond lengths [Å] for Sr atoms in LT and HT $SrMgF_4$ structures

LT phase		Sr5-F1(vi)	2.691(2)
Sr1-F5	2.376(3)	Sr6-F21	2.421(3)
Sr1-F24(i)	2.439(3)	Sr6-F3(vii)	2.495(3)
Sr1-F3	2.456(3)	Sr6-F20	2.497(3)
Sr1-F10	2.481(3)	Sr6-F4(vii)	2.538(3)
Sr1-F16	2.482(3)	Sr6-F19	2.568(3)
Sr1-F11(ii)	2.524(3)	Sr6-F6(vii)	2.716(3)
Sr1-F8	2.654(3)	Sr6-F17	2.757(3)
Sr2-F5	2.440(3)	Sr6-F2(vii)	2.758(3)
Sr2-F4	2.455(2)	Sr6-F23(viii)	2.844(2)
Sr2-F10	2.457(3)	Sr6-F1 (vii)	2.896(3)
r2-F24(iii)	2.523(3)	**Symmetry information:**	
Sr2-F11	2.536(3)	(i) 1-x, y-1/2, -z;	
Sr2-F13	2.606(2)	(ii) x, y, z-1;	
Sr2-F12	2.623(2)	(iii) 1-x, y-1/2, 1-z;	
Sr3-F9	2.454(3)	(iv) x, y, z+1;	
Sr3-F10	2.462(3)	(v) x-1, y, z;	
Sr3-F8	2.484(3)	(vi) 1-x, y+1/2, -z;	
Sr3-F22	2.532(3)	(vii) 1-x, y+1/2, 1-z;	
Sr3-F18	2.545(3)	(viii) 1+x, y, z.	
Sr3-F19	2.577(2)		
Sr3-F14	2.647(3)	**HT phase**	
Sr3-F20	2.655(2)	Sr(1)-F(3) (i)	2.462(8)
Sr3-F15	2.663(3)	Sr(1)-F(1)	2.478(7)
Sr4-F9	2.485(3)	Sr(1)-F(1) (ii)	2.478(7)
Sr4-F11	2.503(2)	Sr(1)-F(3) (iii)	2.526(6)
Sr4-F18(iv)	2.508(3)	Sr(1)-F(3) (iv)	2.526(6)
Sr4-F8 (iv)	2.531(3)	Sr(1)-F(4) (iv)	2.669(11)
Sr4-F19	2.548(3)	Sr(1)-F(2) (v)	2.760(5)
Sr4-F15	2.738(2)	Sr(1)-F(2) (vi)	2.760(5)
Sr4-F14(iv)	2.742(3)	Sr(1)-F(1) (i)	2.941(7)
Sr4-F23	2.780(3)	**Symmetry information:**	
Sr4-F7	2.951(3)	(i) -x+1/2,-y+1/2,z-1/2;	
Sr4-F17(v)	3.187(3)	(ii) x-1,y,z;	
Sr5-F21(ii)	2.386(3)	(iii) x-1,y,z-1;	
Sr5-F18	2.462(3)	(iv) x,y,z-1;	
Sr5-F20	2.489(3)	(v) -x+1,-y+1,z-1/2;	
Sr5-F3(vi)	2.534(3)	(vi) -x,-y+1,z-1/2;	
Sr5-F4(vii)	2.562(3)	(vii) x+1,y,z;	
Sr5-F7(vii)	2.569(3)	(viii) -x+1,-y+1,z+1/2;	
Sr5-F2(vii)	2.607(2)	(ix) x+1,y,z+1;	
Sr5-F24	2.665(3)	(x) x,y,z+1;	
Sr5-F4(vii)	2.562(2)	(xi) -x+1/2,-y+1/2,z+1/2;	
Sr5-F7(vii)	2.569(3)	(xii) x,-y+1,z+1/2.	

Table 2. *Ab initio* calculated linear (refractive indices, birefringence) and nonlinear optical (SHG coefficients) properties for LT and HT phases of SMF.

		LT phase		HT phase	
		hν= 1.165 eV (λ=1064 nm)	2.33 eV (532 nm)	1.165 eV (1064 nm)	2.33 eV (532 nm)
Linear optical properties	n_x	1.4278	1.4330	1.4409	1.4422
	n_y	1.4408	1.4463	1.4231	1.4281
	n_z	1.4438	1.4493	1.4366	1.4465
	Δn	0.0160	0.0163	0.0178	0.0184
SHG coeffficents (pm/V)		d_{21} = 0.022		d_{31} = -0.021	
		d_{22} = 0.044		d_{32} = -0.009	
				d_{33} = -0.078	

Table 3. The components of the polarizability tensor α_{ij} for LT and HT phases of $MgSrF_4$ (Unit: 10^{-24} cm^3)

LT $MgSrF_4$					
Dynamic (optical) polarizability ($\omega \rightarrow \infty$)			Static polarizability ($\omega = 0$)		
86.58	0.00	0.01	960.79	0.00	61.67
0.00	90.18	0.00	0.00	672.11	0.00
0.01	0.00	91.10	61.67	0.00	473.58
HT $MgSrF_4$					
Dynamic (optical) polarizability ($\omega \rightarrow \infty$)			Static polarizability ($\omega = 0$)		
15.31	0.00	0.00	75.65	0.00	0.00
0.00	14.36	0.00	0.00	174.71	0.00
0.00	0.00	14.98	0.00	0.00	82.29

Fig.1. Single crystal $MgSrF_4$ sample, 2 mm thick.

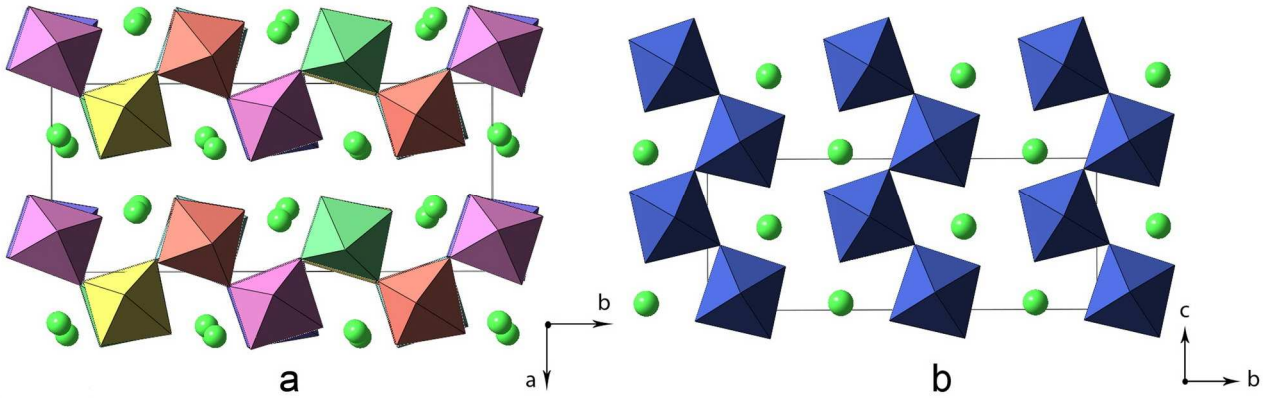

Fig.2. The structure of $SrMgF_4$: low-temperature (a) and high-temperature (b) phases. Green spheres are Sr ions located among the MgF_6 polyhedrons. Different color of MgF_6 octahedrons in section (a) show that they are turned each other and are crystallographically nonequivalent.

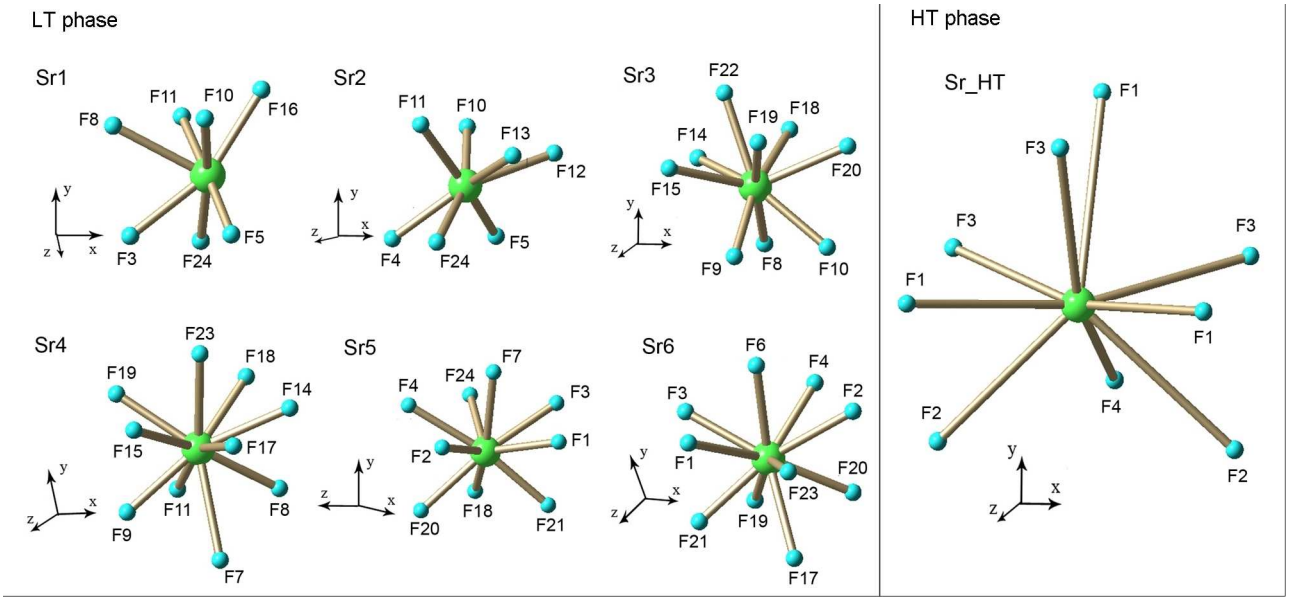

Fig.3. The coordination of Sr ions in LT and HT $SrMgF_4$ structures.

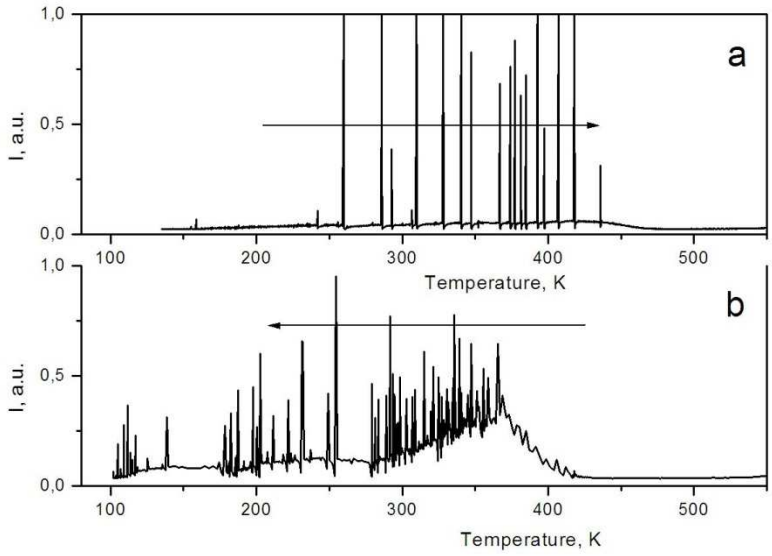

Fig. 4. Spontaneous emission (PEL) in SMF crystals at heating (a) and cooling (b). Heating / cooling rate β is about 20 K/min.

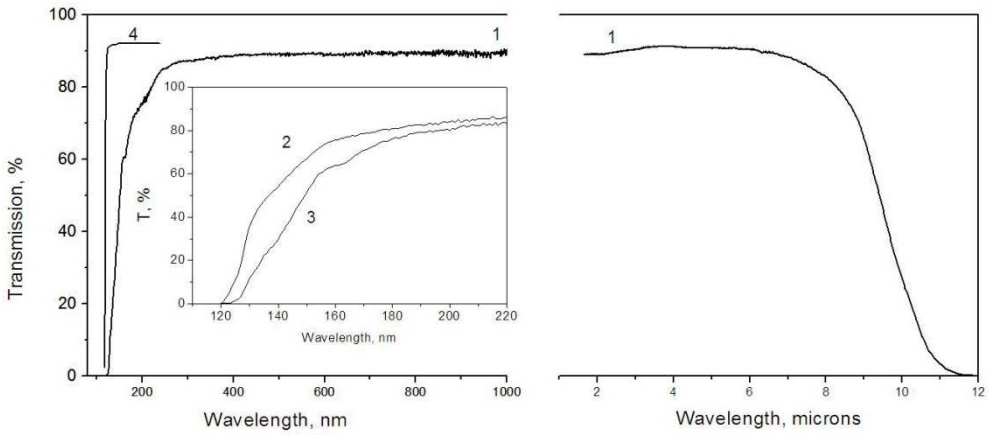

Fig. 5. Transmission spectrum in the VUV to mid-IR spectral range for a low-temperature MSF phase at T=300 K. d=1.2 mm. In the insert: Detail in the shortwave range for SMG plates 0.5 mm and 1.2 mm thick: curves 2 and 3, respectively. 4-shows transmission spectrum for 1 mm thick SMF plate, reconstructed from the reflection spectrum supposing only excitonic absorption near the fundamental absorption edge, without any features related to defects.

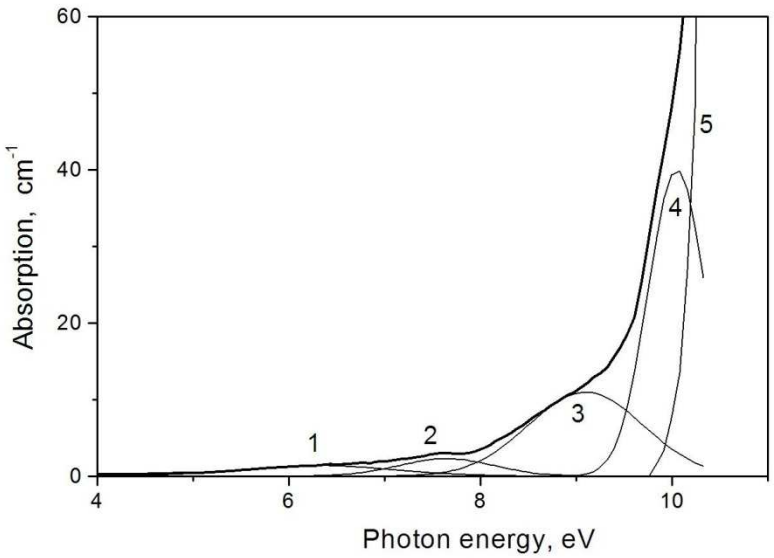

Fig. 6. Decomposition of the room-temperature absorption spectrum for LT-SMF near the fundamental absorption edge: there are 4 gaussians centered at 6.3, 7.65, 9.1 and 10.05 eV (curves 1-4) whereas (5) shows an intense absorption in the excitonic band.

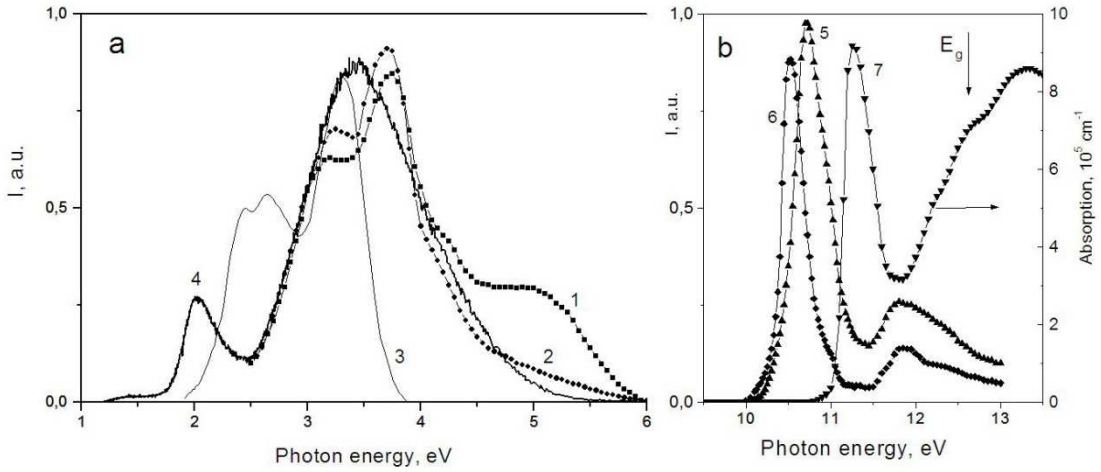

Fig. 7. (a) PL spectra for LT phase of $SrMgF_4$ at 10.6 eV (1), 10.8 eV (2) and 3.8 eV (3) excitations. The XL spectrum is given for comparison (4). (b) PLE spectra for 3.6 eV and 4.8 eV emissions are shown by (5) and (6) curves, respectively. Spectra 1-2, 5-6 are taken from [10]. Absorption spectrum (7) was reconstructed from the reflection spectrum in [10]. Spectra (1-2, 5-6) were recorded at 10 K, whereas spectra (3, 4) were recorded at 300 K. The arrow shows the band gap E_g=12.5 eV in SMF.

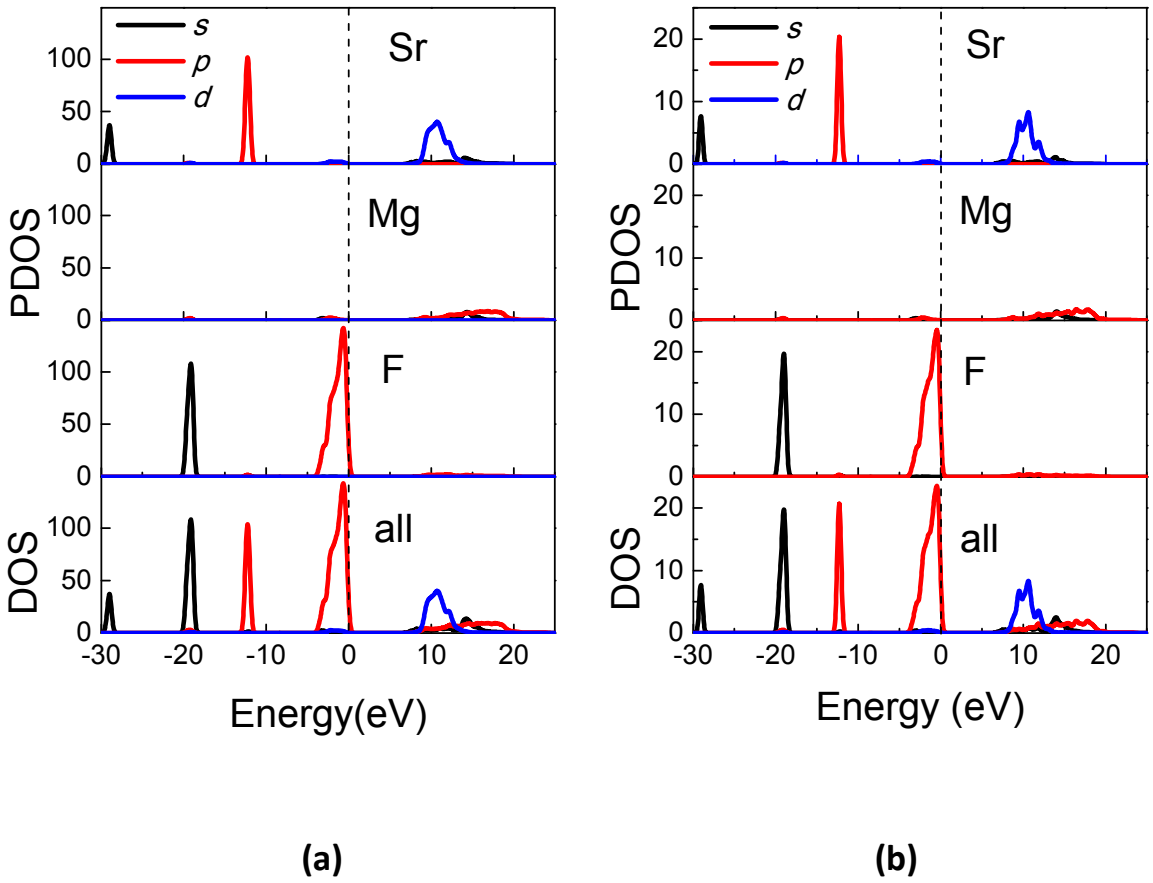

Fig.8. DOS and PDOS projected on constitutional species of atoms in (a) LT phase and (b) HT phase of $SrMgF_4$ (Unit: electrons/eV). The vertical dashed lines indicate the valence band maximum.

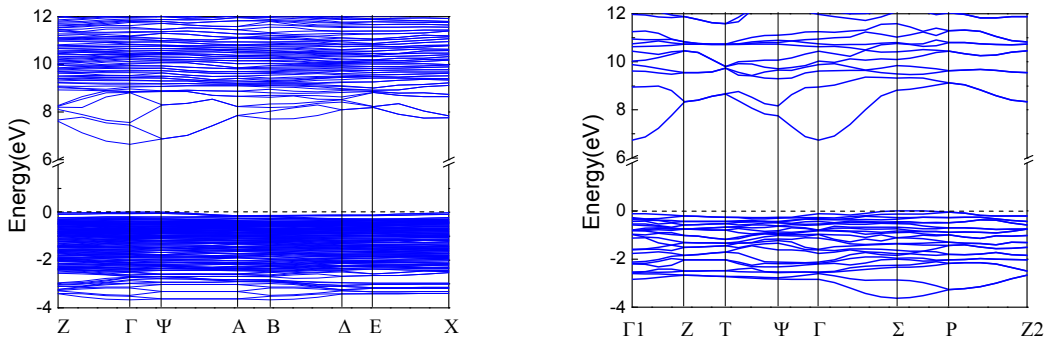

Fig.9. Comparison of the electronic band structure along the lines of high symmetry points in the Brillouin zone for (a) LT phase and (b) HT phase of $SrMgF_4$.

TOC image